Systemic Inflammation Disrupts the Developmental Program of White Matter

Article *in* Annals of Neurology · October 2011

DOI: 10.1002/ana.22489 · Source: PubMed

14 authors, including:

Geraldine Favrais
CHU de Tours, Université François-Rabelais, Tours, France
54 PUBLICATIONS **864** CITATIONS
SEE PROFILE

Yohan van de Looij
University of Geneva
47 PUBLICATIONS **966** CITATIONS
SEE PROFILE

Bobbi Fleiss
RMIT University
142 PUBLICATIONS **1,854** CITATIONS
SEE PROFILE

Nélina Ramanantsoa
French Institute of Health and Medical Research
38 PUBLICATIONS **1,181** CITATIONS
SEE PROFILE

Systemic Inflammation Disrupts the Developmental Program of White Matter

Géraldine Favrais, MD, PhD,[1,2,3,4] Yohan van de Looij, PhD,[5,6] Bobbi Fleiss, PhD,[7] Nelina Ramanantsoa, PhD,[1,2,3] Philippe Bonnin, MD, PhD,[2,3,4,5,6,7,8] Gisela Stoltenburg-Didinger, MD,[9] Adrien Lacaud, BS,[10] Elie Saliba, MD, PhD,[4] Olaf Dammann, MD,[11,12,13] Jorge Gallego, PhD,[1,2,3] Stéphane Sizonenko, MD, PhD,[5] Henrik Hagberg, MD, PhD,[7,14] Vincent Lelièvre, PhD,[1,2,3,9] and Pierre Gressens, MD, PhD[1,2,3,14]

Objective: Perinatal inflammation is a major risk factor for neurological deficits in preterm infants. Several experimental studies have shown that systemic inflammation can alter the programming of the developing brain. However, these studies do not offer detailed pathophysiological mechanisms, and they rely on relatively severe infectious or inflammatory stimuli that most likely do not reflect the levels of systemic inflammation observed in many human preterm infants. The goal of the present study was to test the hypothesis that moderate systemic inflammation is sufficient to alter white matter development.
Methods: Newborn mice received twice-daily intraperitoneal injections of interleukin-1β (IL-1β) over 5 days and were studied for myelination, oligodendrogenesis, and behavior and with magnetic resonance imaging (MRI).
Results: Mice exposed to IL-1β had a long-lasting myelination defect that was characterized by an increased number of nonmyelinated axons. They also displayed a reduction of the diameter of the myelinated axons. In addition, IL-1β induced a significant reduction of the density of myelinating oligodendrocytes accompanied by an increased density of oligodendrocyte progenitors, suggesting a partial blockade in the oligodendrocyte maturation process. Accordingly, IL-1β disrupted the coordinated expression of several transcription factors known to control oligodendrocyte maturation. These cellular and molecular abnormalities were correlated with a reduced white matter fractional anisotropy on diffusion tensor imaging and with memory deficits.
Interpretation: Moderate perinatal systemic inflammation alters the developmental program of the white matter. This insult induces a long-lasting myelination deficit accompanied by cognitive defects and MRI abnormalities, further supporting the clinical relevance of the present data.

ANN NEUROL 2011;70:550–565

The persistently high incidence of neurological adverse outcomes after preterm birth[1] warrants an intensified search for neuroprotective options. Designing such neuroprotectants requires a detailed knowledge of clinical phenotype and pathophysiology.

Major changes have recently been observed in the panorama of brain damage and neurological consequences observed in preterm infants. At the clinical level, severe motor deficits are less frequent,[2] whereas fine motor deficits, cognitive and learning impairments, behavioral disturbances, and sensory deficits have become more prominent.[3] At the structural level, cystic periventricular leukomalacia is less frequent than subtle white matter abnormalities.[4] On the pathophysiologic level, the purely

View this article online at wileyonlinelibrary.com. DOI: 10.1002/ana.22489

Received Sep 23, 2010, and in revised form May 11, 2011. Accepted for publication May 13, 2011.

Address correspondence to Dr Gressens, Inserm U676, Hôpital Robert Debré, 48 Blvd Serurier, F-75019 Paris, France. E-mail: pierre.gressens@inserm.fr

From the [1]Inserm U676, Paris, France; [2]Denis Diderot Faculty of Medicine, University of Paris 7, Paris, France; [3]PremUP, Paris, France; [4]Department of Pediatric and Neonatal Reanimation, Clocheville Hospital, Unversity Hospital Center of Tours, François Rabelais University, Tours, France; [5]Division of Child Development and Growth, Department of Pediatrics, University of Geneva, Geneva, Switzerland; [6]Laboratory for Functional and Metabolic Imaging, Lausanne Federal Polytechnic School, Lausanne, Switzerland; [7]Perinatal Center, Department of Physiology and Neuroscience, Sahlgrenska Academy, Gothenburg University, Goteborg, Sweden; [8]Inserm, U965, Paris, France; [9]Institute of Cell Biology and Neurobiology, Charité University Clinic, Berlin, Germany; [10]CNRS UPR3212, University of Strasbourg, Strasbourg, France; [11]Department of Newborn Medicine, Floating Hospital for Children at Tufts Medical Center, Boston, MA; [12]Perinatal Neuroepidemiology Unit, Hannover Medical School, Hanover, Germany; [13]Neuroepidemiology Unit, Children's Hospital, Boston, MA; and [14]Institute for Reproductive and Developmental Biology, Imperial College, Hammersmith Campus, London, United Kingdom.

Additional supporting information can be found in the online version of this article.

hypoxic–ischemic paradigm has been replaced by a multifactorial hypothesis where systemic inflammation appears to play a key role.[5]

Most epidemiologic studies suggest a strong association between fetal infection/inflammation (chorioamnionitis) and brain damage, especially white matter injury, in the premature newborn and neurological disability in survivors,[6] although a few studies did not confirm this association.[7,8] Experimental studies suggest a sensitizing effect of systemic inflammation that makes the perinatal brain more vulnerable to hypoxic–ischemic or excitotoxic insults.[9,10]

In addition, relatively low levels of systemic inflammation even in the absence of a second insult may alter the programs of brain development, which will result in lasting neurological deficits without leading to frank brain lesions.[11,12] Indeed, systemic infection/inflammation during pregnancy can induce brain abnormalities in offspring, including diffuse white matter cell death after injection of *Escherichia coli* to pregnant rabbits,[13] myelin defects and loss of interneurons after injection of pregnant mice with *Ureaplasma parvum*,[14] and myelination defects in offspring of pregnant rats injected with lipopolysaccharide (LPS).[15]

Although such research provides the proof of concept that systemic inflammation can alter the programming of the developing brain, it does not clarify pathophysiological mechanisms, or provide imaging or behavioral data that allow for a link to the human situation. Furthermore, studies have employed infectious or inflammatory stimuli that are probably much more severe than those observed in most human preterm infants.

Our goal was to test the hypothesis that mild systemic inflammation induced by intraperitoneal injections of interleukin-1β (IL-1β) is sufficient to disrupt oligodendrocyte maturation, myelin formation, and axonal development in newborn mice. In addition, we hypothesized that these white matter changes would lead to later diffusion tensor imaging (DTI) abnormalities and cognitive defects similar to those observed in human preterm infants. Finally, we wanted to elucidate molecular mechanisms related to the transcription of genes controlling oligodendrogenesis, myelin formation, and/or axonal maturation.

Materials and Methods

Animals and Drug Administration

Experimental protocols were approved by the institutional review committee and were carried out in accordance with the Guide for the Care and Use of Laboratory Animals of the National Institutes of Health (NIH).

Sex was determined at birth, and confirmed by abdominal examination at sacrifice. To avoid any potential variability linked to sex differences, only male Swiss pups were used. A 5μl volume of phosphate-buffered saline (PBS) containing 10μg/kg/injection of recombinant mouse IL-1β (R&D Systems, Minneapolis, MN) or of PBS alone (control) was injected intraperitoneally (i.p.) twice a day on days P1 to P4 and once a day on day P5. A second group of pups was similarly treated with IL-1β or PBS between P6 and P10.

The timing of IL-1β injections was chosen to mimic a chronic exposure to circulating cytokines at a developmental stage corresponding to human preterm (P1–P4) and term birth (P6–P10). The dose of injected IL-1β was selected on the basis of what was previously shown to be sufficient to induce sensitization to a secondary excitotoxic insult in newborn mice.[10] Supplementary Figure 1 gives a schematic timeline of the experimental protocol and performed analyses.

Physiological Parameters Assessment

BODY WEIGHT. All litters were culled to 8 pups on the day of birth by random selection. Each pup was weighed daily before physiological tests.

BODY TEMPERATURE. Body temperature was measured by placing a thermocouple probe at the level of the interscapular region, which contains heat-producing brown adipose tissue. Furthermore, brain temperature was measured by inserting a needle thermocouple microprobe (52-1666; Harvard Apparatus, Holliston, MA) through the skull to a depth of 2mm inside the brain.

BREATHING VARIABLES. Breathing variables were measured noninvasively at P5, 1 hour after the last injection, using a battery of 4 whole-body flow barometric plethysmographs allowing the simultaneous measurement of breathing variables as previously described.[16] Each plethysmograph was composed of two 50ml Plexiglas chambers, which were immersed in a water bath set that maintained their temperature at 33°C. A 200ml per minute flow of dry air (Brooks airflow stabilizer, Urlo, Holland) was divided into two 100ml per minute flows through the chambers. The differential pressure between the chambers (DRUCK-EFFA transducer, Asnières, France) was filtered (bandwidth, 0.15–20 Hz at −3dB), converted into a digital signal at a sampling rate of 100Hz, and processed (Labview; National Instruments, Austin, TX). Calibration was done before each session using a built-in pump incorporating a microsyringe (Ito Corporation, Fuji, Japan), which injected a sinusoidal airflow with maximal amplitude of 2μl and frequency of 8Hz into the animal chamber. The limitations of the plethysmographic method in newborn mice have been discussed elsewhere.[17] Because of these limitations, the absolute values of tidal volume (V_T) and ventilation (V_E) are indicative only, whereas breath duration absolute values (T_{TOT}) and apnea durations are reliable. T_{TOT} (seconds (sec)), V_T (μl/g), and V_E (calculated as $V_T \cdot T_{TOT}^{-1}$ and expressed in μl/sec/g) were calculated during apnea-free periods. Apneas were defined as ventilatory pauses longer than twice the duration of the preceding breath.[18] Following a 2-minute period of familiarization in the plethysmograph chamber, breathing variables were recorded for 10 minutes, and averaged over this period.

HEART RATE. The plethysmographic chambers were equipped with recording platforms composed of 4 rectangular gold electrodes insulated from each other and embedded in the floor of the chamber, as previously described.[19] Conduction was enhanced using electrode hydrogel (Sekisui Plastics Company, Nara, Japan). The signals were digitized at a sample rate of 1000 Hz (16 bits, PCI-6229, National Instruments). An electrocardiographic (ECG) signal was obtained when at least 3 paws contacted 3 electrodes and, occasionally, when the pup laid on the floor. Heart rate was determined from the R-R wave peaks after visual selection of continuous, 1-second or longer ECG segments with clearly defined QRS waves. Heart rates were averaged over the entire recording period.

BLOOD GASES AND HEMOGLOBIN. $PaCO_2$, pH, bicarbonate (HCO_3^-), and hemoglobin were analyzed on P5 mice, immediately after the baseline ventilation measurement, using a clinical blood gas analyzer (ABL80; Radiometer America, Cleveland, OH). The pups were decapitated, and the blood samples were collected from the neck in heparinized capillary tubes and immediately analyzed, as previously described in infant rats.[20]

Cerebral Arterial Blood-Flow Monitoring by Color-Coded Pulsed Doppler Ultrasound Imaging

P5 mice were subjected to ultrasound measurements using an echocardiograph (Vivid 7; GE Ultrasound, Horten, Norway) equipped with a 12MHz linear transducer (12L) as previously reported.[21] With the ultrasound device applied on the occipital part of the head, a medial sagittal cross-sectional view gave access to the basilar trunk, a parasagittal cross-sectional view to the right or left intracranial internal carotid arteries just at their emergence through the base of the skull. Arteries were localized by color-coded Doppler imaging and revealed by a red color Doppler signal. A pulsed Doppler sample was then placed on the longitudinal axis of each vessel upstream from the circle of Willis. Spectral analysis of the Doppler signal was then recorded with an optimal angle correction of the Doppler beam. Heart rate, peak systolic, end diastolic, and time-average mean blood flow velocities were measured from the recorded blood flow velocity waveforms.

Behavioral Assessment

All mice were weaned at P25. Their global psychomotor functions were evaluated in an open field paradigm, performed at P28. Animals were placed in a 36 × 36 × 10cm arena with a $6cm^2$ grid floor, located in a quiet room with lights dimmed. Their activities were recorded for 10 minutes. Locomotor activities (ie, outer, inner, and total squares crossed per minute), general behavior (ie, freezing and grooming times), and the number of jumps were assessed during 10 minutes of recorded activities.

Temporal and spatial memory functions were assessed at P29 and P30 through the novel object recognition (NOR) and the object location memory (OLM) tests, respectively. For these tests, the exploration time of 2 objects placed in a 36 × 36 × 10cm square arena was measured twice for 4 minutes, 30 minutes apart. First, 2 identical objects were placed in 2 distinct corners of the box. Second, 1 of the 2 cues was either displaced or replaced by a new cue for OLM or NOR assessments, respectively. Exploration time was defined as the duration an animal spent either pointing its nose toward the object at a distance of <1cm and/or touching it with the nose, whereas turning around, climbing, and sitting on a cue were not considered as exploration. Recognition of the familiar object was scored by preferential exploration of the novel object using a discrimination index (novel object interaction/total interaction with both objects, range from 0 to 100%; 50% = no preference).

DTI

Mice treated with IL-1β or PBS between P1 and P5 were sacrificed at P35. Brains were fixed in 4% paraformaldehyde. Ex vivo magnetic resonance imaging (MRI) analyses were performed on an actively shielded 9.4T/31cm magnet (Magnex Scientific, Abington, UK) interfaced to an INOVA console (Varian, Palo Alto, CA) with 12cm gradient coils (400mT/m, 120 milliseconds) with a transceiver 25mm birdcage radiofrequency coil. Spin-echo sequence with addition of the Stejskal-Tanner diffusion gradients was used. A dual gradient diffusion gradient sampling scheme was used as well as the 6 opposite directions to cancel b value cross terms. Intensity, duration, and diffusion time were set to 22G/cm, 3 milliseconds, and 19 milliseconds, respectively, given a b value of $1{,}185s/mm^2$. A field of view of 20 × $20mm^2$ was sampled on a 128 × 128 Cartesian grid, given an in-plane pixel size of 156μm, then zero-filled to 256 × 256. Twenty slices of 0.8mm thickness were acquired in the axial plane. Scan were averaged 6× with echo time and repetition time = 30 and 5,000 milliseconds, respectively. Using Matlab software (Mathworks, Natick, MA), diffusivity values (apparent diffusion coefficient [ADC], axial diffusivity [$D_{//}$], and radial diffusivity [$D_{\perp}$]) as well as fractional anisotropy (FA) were derived from the tensor. To maximally avoid partial volume effect, regions of interests were delimited on direction encoded color maps in the corpus callosum (CC), cingulum (Cg), external capsule (EC), superficial layers of the motor cortex (Cx), and basal ganglia (BG) at 4 different image planes from the splenium to the genu of the CC (Fig 1). Diffusivity as well as FA values were averaged on these 4 different image planes to obtain 1 data set per structure (CC, Cg, EC, and Cx) for each mouse.

Immunohistochemistry, Immunofluorescence, and Bodian-Luxol Staining

Primary antibodies used for immunohistochemistry and immunofluorescence are listed in Supplementary Table 1. A counterstain by DAPI (1:10,000; Sigma-Aldrich, St Louis, MO) labeling the nucleus was performed at the end of the immunofluorescence protocol.

After the intervention, brains were collected at P5, P10, P15, and P30. For paraffin sections, brains were immersed immediately after sacrifice in 4% formaldehyde for 4 days at room temperature, prior to dehydration and paraffin embedding. For frozen sections, mice were intracardially perfused with 4% paraformaldehyde–0.12M phosphate buffer solution under

isoflurane anesthesia. Brains were then postfixed in 4% paraformaldehyde overnight at 4°C. After 2 days in 10% sucrose–0.12M phosphate buffer solution, brains were embedded in 10% sucrose–7.5% gelatin solution before freezing at −80°C for storage until sectioning on a cryostat. Immunohistochemistry, immunofluorescence, and Bodian-Luxol staining were performed as previously described.[22,23]

The intensity of the myelin protein immunostainings was assessed by a densitometry analysis through NIH ImageJ Software. Optical density was deduced from grayscale standardized to the photomicrograph background. Four measurements per brain (2 in each hemisphere) were performed in each assessed brain region. Cell counts were performed in duplicate by a blinded experimenter within a defined brain structure on 4 sections per animal through NIH ImageJ Software. Results are expressed as positive cells per square millimeter.

Electron Microscopy and Analysis

Mice treated with IL-1β (n = 3) or PBS (n = 3) between P1 and P5 were sacrificed at P30 by intracardial perfusion with 2% paraformaldehyde–0.25% glutaraldehyde for 10 minutes under anesthesia by inhaled isoflurane. Brains were postfixed overnight in 4% paraformaldehyde at 4°C, and the Cg regions were cut coronally to obtain 100μm-thick sections. The region of interest was located after toluidine blue staining. Then, ultrathin sections were processed for transmission electron microscopy by standard procedures.

The myelinated axon diameter was measured on axons that were cut coronally. Three areas were explored for each animal, and an average of 200 measurements of myelinated axon diameter per animal were performed, using NIH Image J software. The thickness of the myelin sheath was assessed by determining the G ratio (axon diameter/total fiber diameter).

Quantitative Reverse Transcription Polymerase Chain Reaction

Cortex and underlying white matter at the level of the anterodorsal sensorimotor cortex were dissected at P0 and, after the i.p. injection schedule, at P5, P10, P15, and P30 in each experimental group. Sample preparations, primer design, and polymerase chain reaction (PCR) protocol were similar to that previously described.[24]

Primer sequences are given in Supplementary Table 2. *GAPDH* (glyceraldehyde-3-phosphate dehydrogenase gene) was chosen to standardize all the quantitative experiments. The differences between samples were calculated as the specific ratio of the gene of interest/housekeeping gene.

Statistical Analysis

Quantitative data are expressed as mean ± standard deviation values for each treatment group. Comparisons of results were conducted by using either nonparametric Mann-Whitney test or a 2-way analysis of variance with Treatment and Time as factors (Prism version 4.01 for Windows; GraphPad Software, San Diego, CA). When a main effect of Treatment or Time was found to be significant, we conducted pairwise comparisons between treatment groups using a Mann-Whitney test.

Results

Intraperitoneal IL-1β–Induced Systemic Inflammation without Altering Survival, Weight, Cerebral Blood Flow, and Brain Anatomy

IL-1β injections between P1 and P5 induced systemic inflammation as demonstrated by increased blood concentration of IL-1β and tumor necrosis factor α (Fig 2A). As previously reported,[10] IL-1β injections between P1 and P5, when compared to PBS injections, had no effect on mortality (which was <1% in both experimental groups and which occurred during the treatment period). At P1, P5, and P30, body weights were similar in both groups (see Fig 2B).

IL-1β injections between P1 and P5 induced a moderate decrease in minute ventilation, mainly due to the increase in breathing cycle duration (see Fig 2). In addition, animals exposed to IL-1β had an increase in apnea duration, although total duration of apneas remained low. These respiratory changes were accompanied by a small increase in blood HCO_3^- but had no significant impact on blood pH, PCO_2, PO_2, hemoglobin, or heart rate. IL-1β administration induced a moderate and transient drop in body and brain temperatures.

By comparison, IL-1β injections between P6 and P10 had no detectable effect on body weight and body temperature (Supplementary Fig 2).

Ultrasound imaging performed in P5 mice on the 3 pre-Willis arteries (2 internal carotid arteries and basilar trunk) did not reveal any difference in systolic, diastolic, or time-average mean blood flow velocities between mice injected with IL-1β or with PBS between P1 and P5 (Supplementary Fig 3). This strongly suggested that IL-1β injections had no detectable impact on cerebral blood flow.

In addition, cresyl violet staining did not reveal any gross anatomical abnormality or destructive lesions in brains of P5[10] and P30 (data not shown) animals exposed to IL-1β between P1 and P5 or between P6 and P10, compared to PBS.

Intraperitoneal IL-1β Altered White Matter Anisotropy and Induced a Long-Term Memory Deficit

At P29 to P30, mice exposed to IL-1β between P1 and P5 showed a severe deficit in memory, as they failed to recognize novel or misplaced objects in NOR and OLM memory tests, respectively (Fig 3A, B and Supplementary Table 3). This cognitive impairment was absent in P29 to P30 mice treated by IL-1β between P6 and P10 (see Fig 3A, B). The memory deficit observed in mice exposed to IL-1β between P1 and P5 was not related to

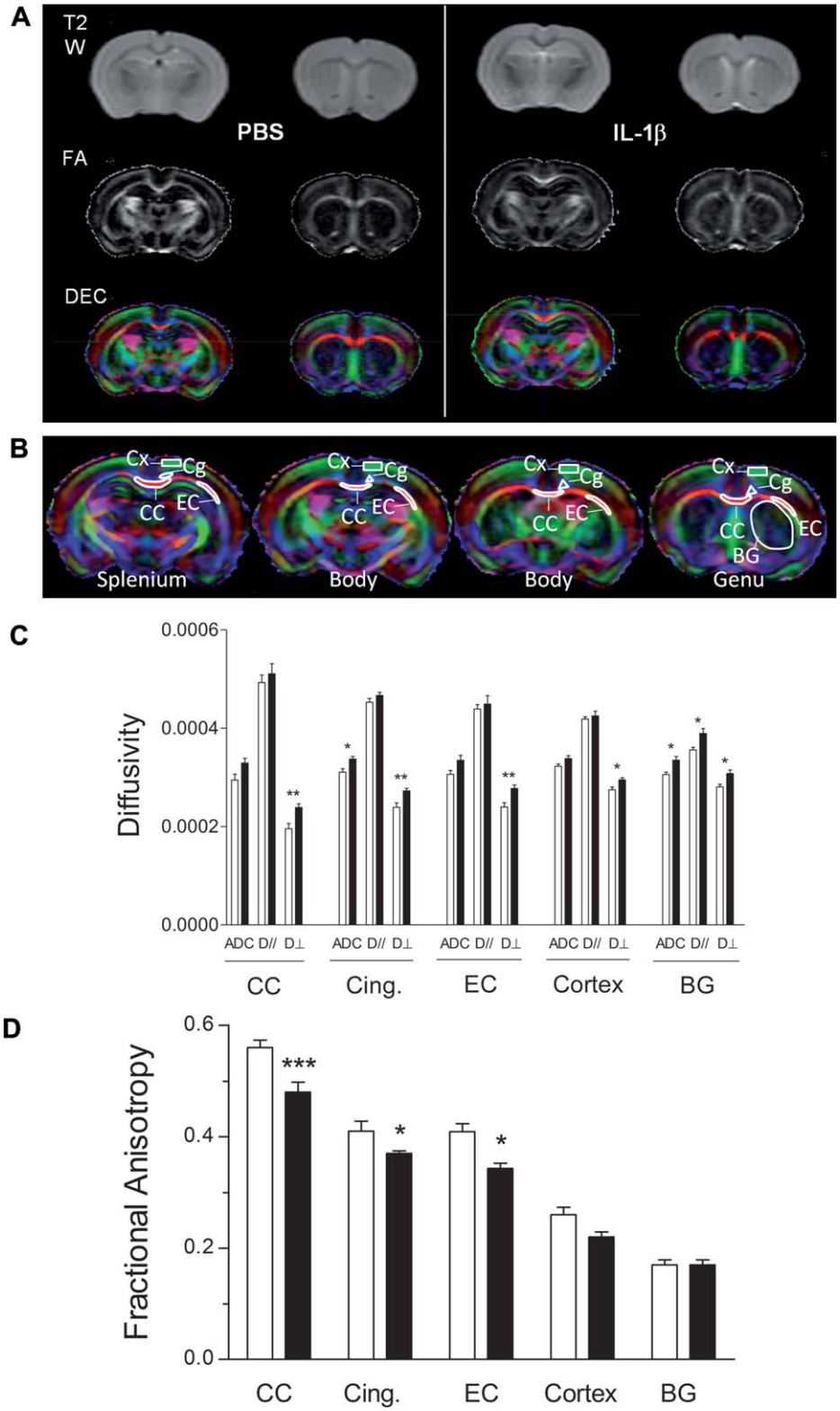

FIGURE 1: The neonatal exposure to interleukin (IL)-1β–induced microstructural abnormalities within the white matter at P35. (A) Magnetic resonance images (T_2W) and diffusion tensor imaging (DTI)-derived maps (fractional anisotropy map [FA], direction encoded color map [DEC]) were obtained from the ex vivo brains of P35 mice subjected to phosphate-buffered saline (PBS) (n = 5) or IL-1β injections (n = 5) from P1 to P5. (B–D) The axial diffusivity ($D_{//}$), the radial diffusivity ($D_{\perp}$), the apparent diffusion coefficient (ADC) (C), and the FA (D) were derived from the DTI data and measured within the corpus callosum (CC), external capsule (EC), cingulum (Cg, Cing.), basal ganglia (BG), and cortex (Cx) in the PBS (n = 5, *white bar*) and the IL-1β (n = 5, *black bar*) groups as demonstrated in B. Results are expressed as mean ± standard deviation. Asterisks indicate statistically significant difference from respective white bar (C, D), *$p < 0.05$, **$p < 0.01$, ***$p < 0.001$ by Mann-Whitney test.

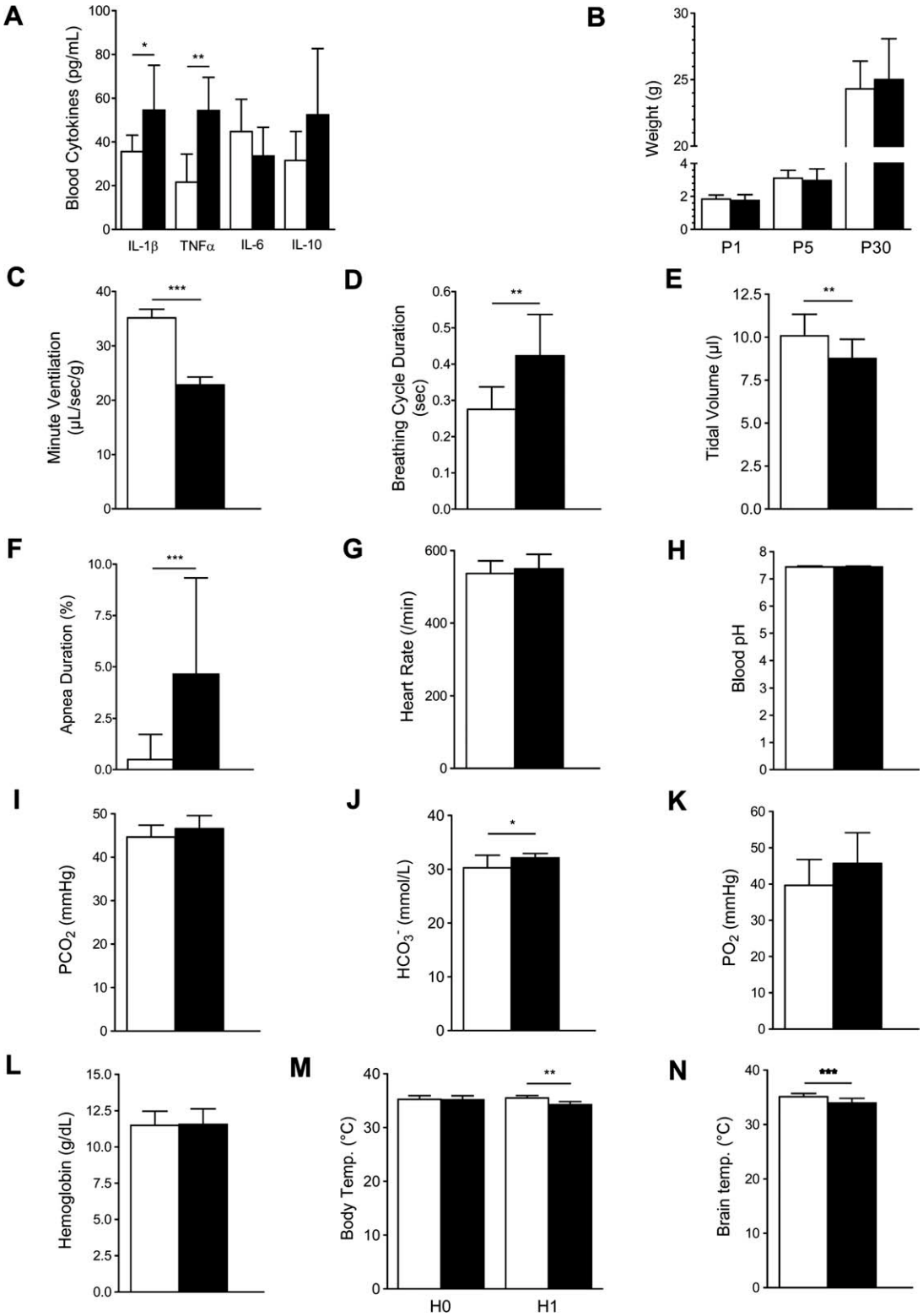

FIGURE 2: Physiological effects of systemic injections of interleukin (IL)-1β. Comparison of mice treated by IL-1β (*black bars*) or phosphate-buffered saline (PBS) (*white bars*) from P1 to P5. (A) Measurement of blood cytokine levels by enzyme-linked immunosorbent assay at P5 (n = 6 for each group). TNF = tumor necrosis factor. (B) Weight gain from birth to adulthood (n = 25 in PBS group and n = 35 in IL-1β group). (C–E) Baseline ventilation measured in plethysmograph at P5, 1 hour after the last injection (n = 23 in PBS group and n = 25 in IL-1β group). (F, G) Apnea duration (F) and mean heart rate (G) calculated over the 10-minute recording of baseline ventilation (n = 23 in PBS group and n = 25 in IL-1β group). (H–L) Blood pH, gases, and hemoglobin measured at P5, immediately after the baseline ventilation measurement (n = 23 in PBS group and n = 25 in IL-1β group). (M) Body temperature measured at interscapular level just before and 1 hour after the last injection at P5 (n = 23 in PBS group and n = 25 in IL-1β group). (N) Brain temperature measured immediately after baseline ventilation measurement (n = 23 in PBS group and n = 25 in IL-1β group). Results are expressed in means ± standard deviation. *$p < 0.05$, **$p < 0.01$, ***$p < 0.001$ by Mann-Whitney test.

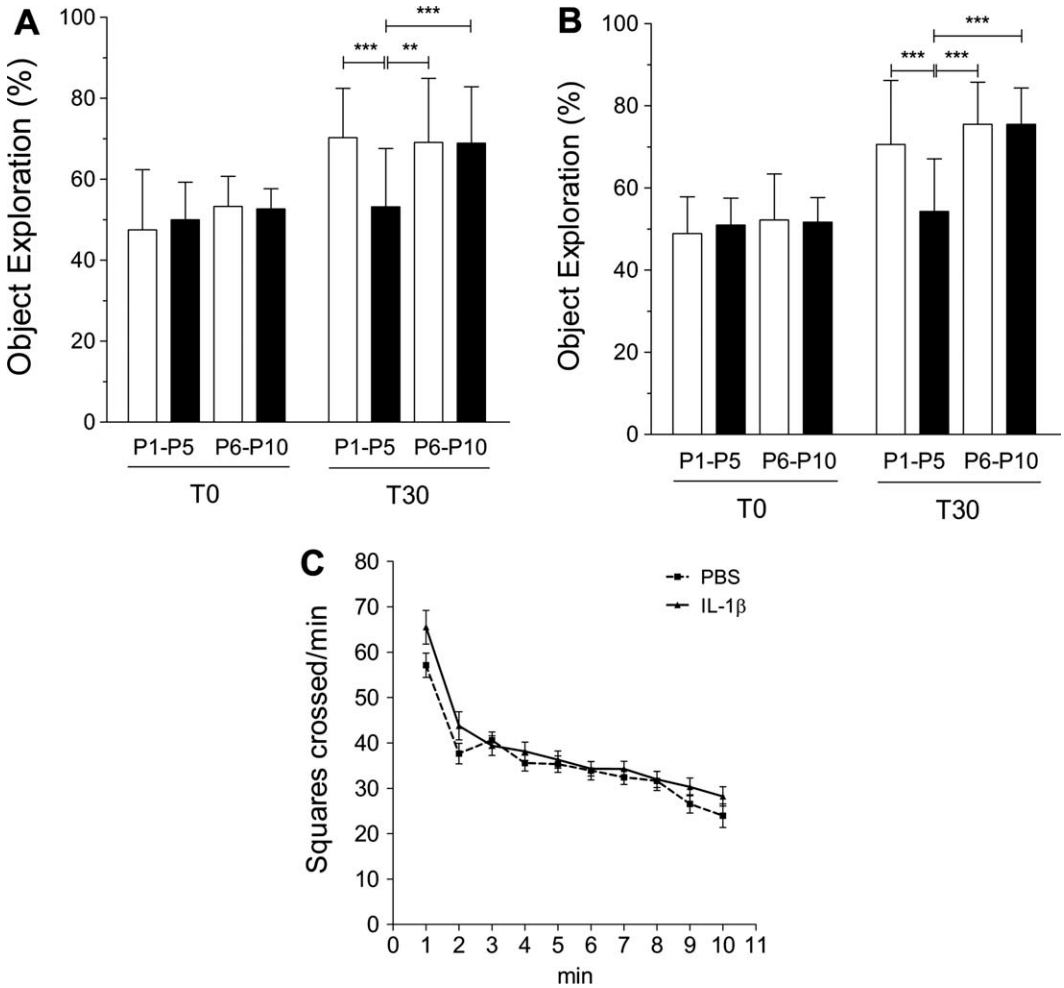

FIGURE 3: The systemic injection of interleukin (IL)-1β from P1 to P5 induced a long-lasting behavioral impairment. (A, B) Mice were subjected to the (A) novel object recognition (NOR) and (B) the object location memory (OLM) tests at P29 and P30. Mice treated with intraperitoneal injections of phosphate-buffered saline (PBS) (*white bars*) or IL-1β (*black bars*) from P1 to P5 (n = 21 and n = 29 for NOR; n = 20 and n = 28 for OLM, respectively) or from P6 to P10 (n = 10 and n = 11 for both tests, respectively) were considered. The time spent to explore 1 object during the first round (T0) and the novel or misplaced object during the second round 30 minutes later (T30) was expressed in percentage of the overall exploration time. Asterisks indicate statistically significant difference in percentage of exploration time between groups during the T30 period: **$p < 0.01$ and ***$p < 0.001$ by nonparametric Mann-Whitney test performed after 2-way analysis of variance. (C) Mice treated with PBS (n = 30, *dotted line*) or IL-1β (n = 41, *solid line*) from P1 to P5 were subjected to the open field test at P28, including the quantification of squares crossed per minute for 10 minutes. Results are expressed as mean ± standard deviation.

FIGURE 4: The systemic injection of interleukin (IL)-1β from P1 to P5 led to a diffuse reduction of the myelin proteins at P15 and P30. (A–D) Immunostainings of 3 major myelin proteins myelin basic protein (MBP), proteolipid protein (PLP), and myelin-associated protein (MAG) were performed on P15 (A–C) and P30 (A–D) brains embedded in paraffin. Mice were treated with phosphate-buffered saline (PBS) or IL-1β from P1 to P5 (A–D) and from P6 to P10 (D) (n = 6 in each group). (A) Photomicrographs of MBP immunostaining of P30 brains at original magnification ×1.5 (*left panel*) and ×40 (*right panel*) focusing on the sensorimotor cortex; scale bars = 2,000μm and 50μm, respectively. (B) Photomicrographs of PLP immunostaining of P30 brains at original magnification ×1.5 (*left panel*) and ×20 (*right panel*) focusing on the white matter; scale bars = 2,000μm and 100μm, respectively. (C) Photomicrographs of MAG immunostaining of P30 brains at original magnification ×1.5 (*left panel*) and ×20 (*right panel*) focusing on the corpus callosum; scale bars = 2,000μm and 100μm, respectively. (D) Photomicrographs of MBP immunostaining focusing on the sensorimotor cortex of P30 mice treated with PBS or IL-1β from P1 to P5 and from P6 to P10; original magnification ×10, scale bar = 20μm. The optical densities of stainings were determined in each experimental condition within the sensorimotor cortex for MBP (A, D), the white matter for PLP (B), and the corpus callosum for MAG (C). White bars = PBS group, black bars = IL-1β group. Results are expressed as means ± standard deviation. Asterisks indicate statistically significant difference from white bar, *$p < 0.05$ and $p < 0.001$ by Mann-Whitney test.

a deficit in exploratory behavior, as these mice performed as PBS controls in the open field test (see Fig 3C).

T_2W sequence analysis of P35 brains exposed to systemic IL-1β between P1 and P5 confirmed the absence of macroscopic abnormalities (see Fig 1A). However, microstructural changes were detected with an increase of the $D_{\perp}$ in the CC, EC, Cg, BG, and Cx, whereas the $D_{//}$ and the ADC were increased in the BG

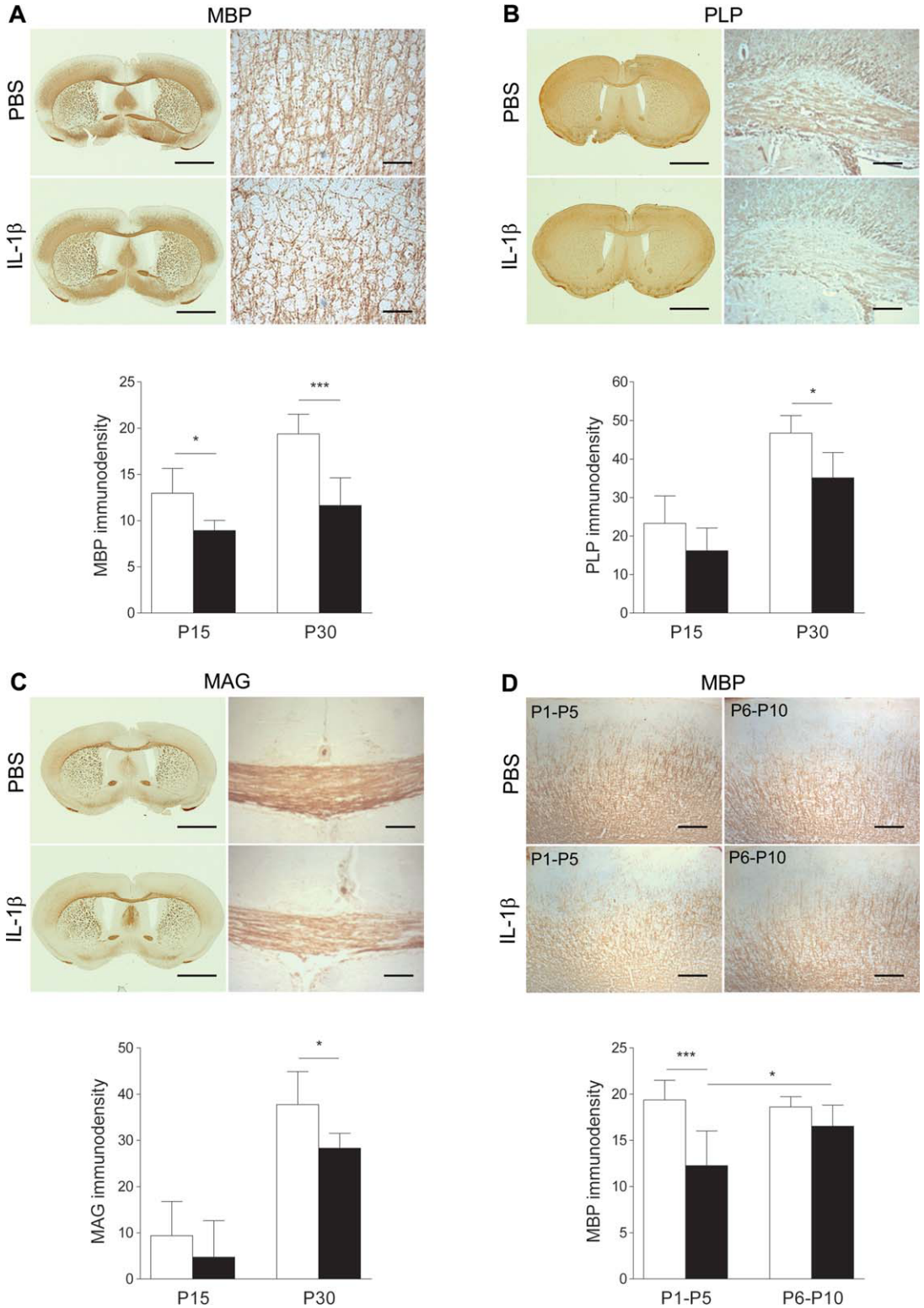

FIGURE 4.

only (see Fig 1A–C). In addition, FA was significantly lower in all white matter structures analyzed: CC and EC as well as Cg of IL-1β animals compared to controls (see Fig 1D). Similar diffusion abnormalities in multiple white matter structures confirmed diffuse white matter injuries in IL-1β mice.

IL-1β–Induced White Matter Alterations Resulted from a Combined Myelinopathy and Axonopathy

To elucidate the mechanisms by which intraperitoneal IL-1β between P1 and P5 could impact white matter, immunohistochemical and electron microscopy studies were performed. Densitometric analysis performed on P15 and P30 brains showed an overall reduction of myelin proteins including myelin basic protein (MBP) (at the level of Cg, cortex and BG), proteolipid protein (PLP) (at the level of Cg, CC, EC, and anterior commissure), and myelin-associated protein (MAG) (at the level of Cg and CC) in IL-1β–treated animals when compared to controls (Fig 4A–C and Supplementary Fig 4). This reduction was time dependent, with a MBP reduction observed as early as P15 and a subsequent PLP and MAG reduction observed at P30 (see Fig 4A-C). This reduction in density of myelin markers was associated with a striking disorganization in the orientation (see Fig 4A) and a reduction of the length of penetration (data not shown) of MBP-positive fibers within the sensorimotor cortex.

Interestingly, MBP density within the sensorimotor cortex of P30 animals treated with IL-1β between P6 and P10 was similar to control levels (see Fig 4D), in keeping with the lack of effects of such a treatment on memory tests.

Bodian-Luxol fast blue staining of P1 to P5 treated brains did not reveal any reduction of axonal density but further confirmed the myelin reduction at P30 (Fig 5). Immunolabeling with SMI-32, a marker of nonmyelinated axons, showed an increased labeling in the IL-1β–exposed animals. Electron microscopy confirmed our observation of fewer myelinated axons in IL-1β–exposed animals. Interestingly, in IL-1β–exposed animals where axons were myelinated, the axons had a normal myelin sheath that appeared appropriately compacted, as confirmed by the G ratio analysis.

We also performed a morphometric analysis of the axonal diameter of myelinated fibers crossing in the Cg (see Fig 5E). This study revealed a reduction in fibers exhibiting the largest axonal diameters (>0.5μm) that was counterbalanced by an increase in numbers of small fibers with diameters between 0.2 and 0.4μm. This reduction in radial axon diameter could result from impaired axonal outgrowth. In support of this hypothesis, we observed a decrease of Wnt7a transcripts (see Fig 5F) encoding a peptide involved in the axonal growth[25,26] at P5 in the IL-1β–treated group. In contrast, no detectable changes were observed in the expression of light and medium chain neurofilament transcripts (see Fig 5G, H).

Interestingly, when IL-1β was injected between P6 and P10, we observed a reduction of the expression of Wnt7a and light chain neurofilament in P10 IL-1β–treated pups, when compared to control pups (Supplementary Fig 5).

IL-1β Impaired Oligodendrocyte Development

The myelination defect observed in the P1 to P5 IL-1β–treated animals could be due to a reduction of mature myelinating oligodendrocytes. Olig2 immunolabeling, a marker of oligodendrocytes irrespective of their stage of maturation, did not reveal any difference between IL-1β–treated animals and controls (Fig 6A). Supporting these data, IL-1β had no detectable effect on the density of cleaved caspase 3-positive cells (a marker of cell death), of Ki67-positive cells (a marker of proliferation), or of Olig2/Ki67 double-positive cells (see Fig 6B–D).

In contrast, IL-1β–treated animals displayed an increased density of NG2- and PDGFRα-positive cells (markers of oligodendrocyte progenitors), but a decreased

FIGURE 5: The systemic injection of interleukin (IL)-1β from P1 to P5 induced a reduction of the axon diameter and ensheathment without altering the myelin sheath morphology. (A) Photomicrographs of Bodian-Luxol histochemistry performed on 10μm- thick paraffin sections within the cingulum of P30 mice treated with phosphate-buffered saline (PBS) or IL-1β from P1 to P5; original magnification ×40 and ×63, scale bars = 20μm and 5μm, respectively. (B) Immunofluorescent staining of SMI-32, a marker of nonmyelinated axons, performed on 10μm-thick frozen sections within the cingulum at P30; original magnification ×40, scale bars = 20μm. (C) Electron microscopy (EM) processed on P30 brains of mice treated with PBS or IL-1β from P1 to P5 focusing on the cingulum; original magnification ×20,000 and ×10,000; scale bars = 1μm and 0.5μm, respectively. (D) Assessment of the myelin sheath thickness in reference to axon diameter by the G ratio measurement (axon diameter/fiber diameter) within the cingulum at P30 (PBS [n = 3, *white bars*] and IL-1β [n = 3, *black bars*]). (E) Classification of myelinated axons according to their diameter (mean, 0.1μm; range, 0–1.2μm; interval, 0.1μm) within the cingulum at P30 (PBS [n = 3, *dotted line*] and IL-1β [n = 3, *solid line*]). Axon diameter was measured on coronally sectioned axons from EM photomicrographs. (F–H) Relative Wnt7a (F), medium neurofilament (NF-M) (G), and light neurofilament (NF-L) (H) expressions by quantitative polymerase chain reaction at P0 (n = 4, *gray bar*) and at P5, P10, P15, and P30 in PBS (n = 4 at each age, *white bars*) and IL-1β (n = 4 at each age, *black bars*) groups within cortex and white matter. Results are expressed as mean ± standard deviation. Asterisks indicate statistically significant difference from white bar (D, F, G, H) or from dotted line (E), *$p < 0.05$ and ***$p < 0.001$ in Mann-Whitney test. ▶

density of O4-positive cells (marker of oligodendrocyte precursors), a decreased expression of CNPase (2′3′cyclic nucleotide 3′ phosphohydrolase, a marker of premyelinating oligodendrocytes), and a reduced density of Adenomatosis Polyposis Coli (APC)-positive cells (a marker of myelinating oligodendrocytes) (Fig 7).

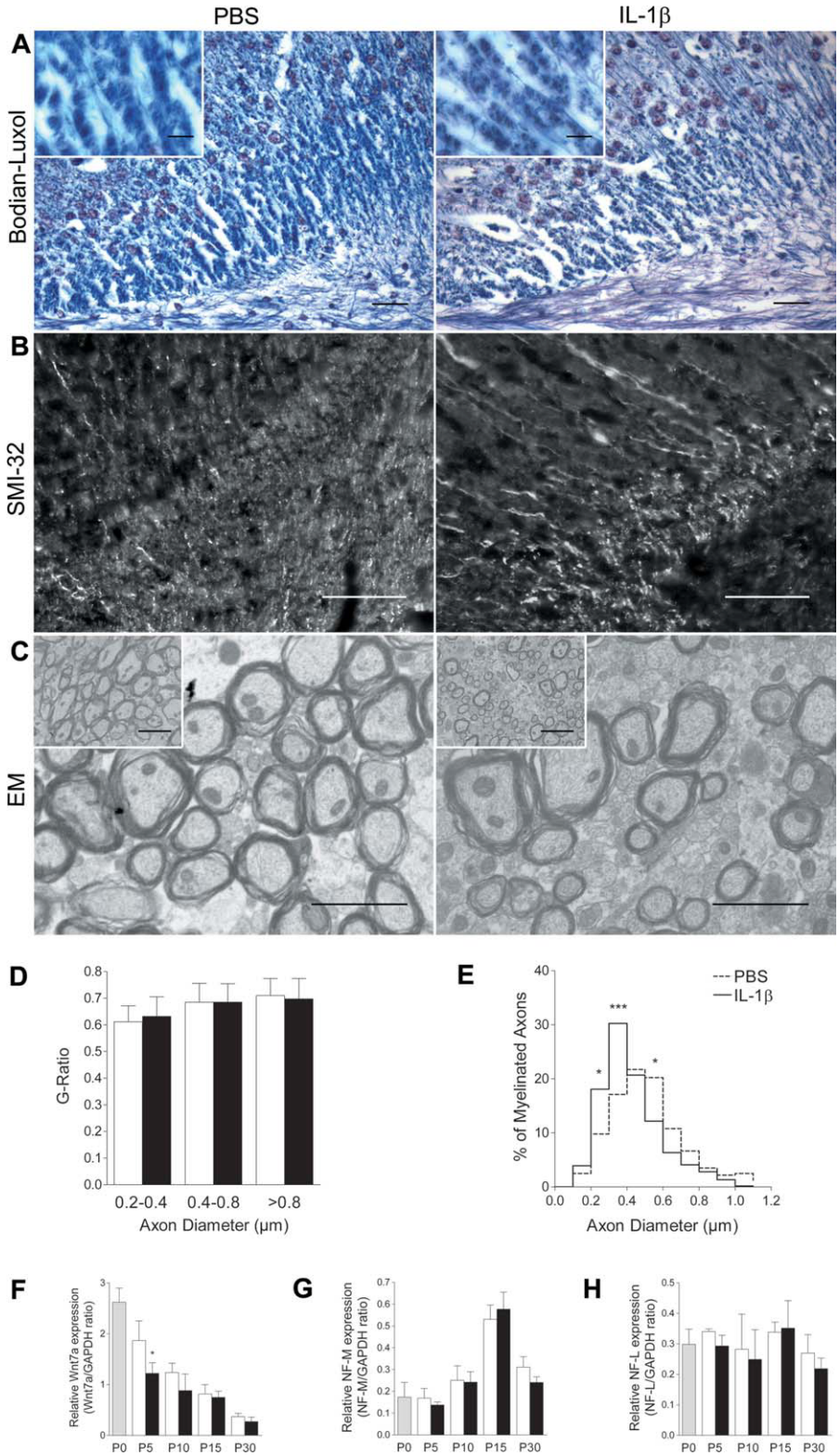

FIGURE 5.

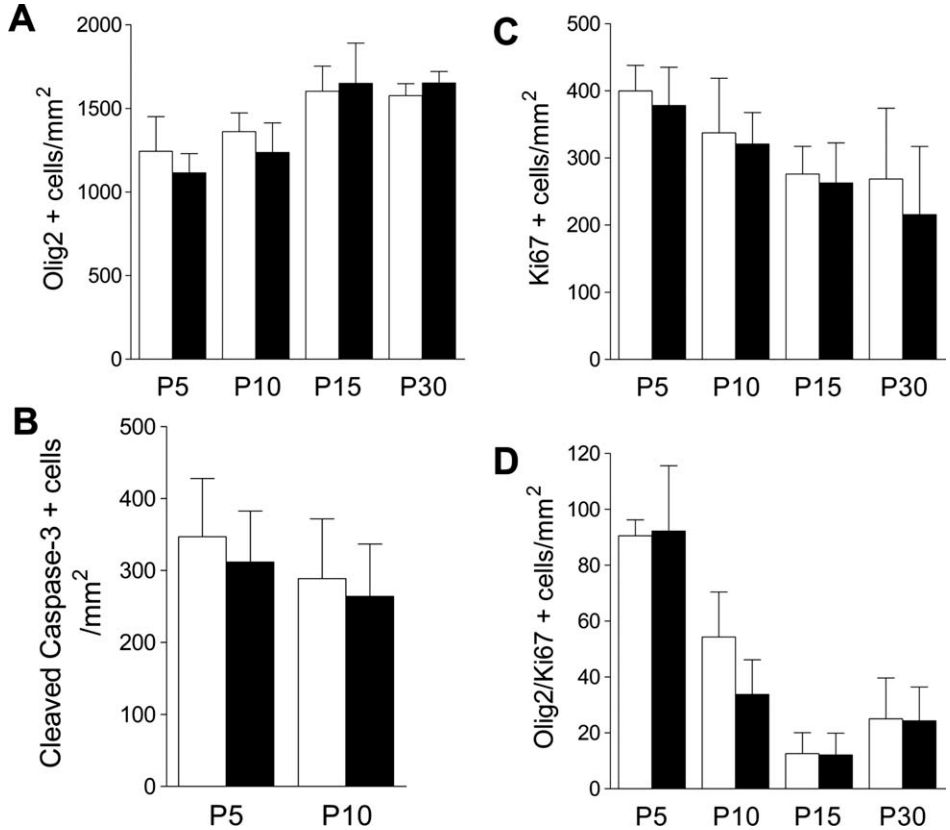

FIGURE 6: The systemic injection of interleukin (IL)-1β from P1 to P5 did not affect the total number of oligodendrocytes, cell death, and proliferation. (A) Quantification of fluorescent Olig2$^+$ cells/mm^2 in the cingulate white matter of mice treated with phosphate-buffered saline (PBS) (n = 6 at each age, *white bars*) or IL1-β (n = 6 at each age, *black bars*) at P5, P10, P15, and P30. Staining was performed on 10μm-thick paraffin sections. (B) Quantification of fluorescent cleaved caspase 3$^+$ cells/mm^2 at P5 and P10 within the cingulate white matter of mice treated with PBS (n = 6 at each age, *white bars*) or IL-1β (n = 6 at each age, *black bars*). Cleaved caspase 3 staining was performed on 10μm-thick frozen sections. (C, D) Quantification of Ki67$^+$ (C) and of double-stained Ki67/Olig2$^+$ (D) cells/mm^2 within the subventricular zone of mice treated with PBS (n = 6 at each age, *white bars*) or IL-1β (n = 6 at each age, *black bars*) at P5, P10, P15, and P30. Stainings were performed on 10μm-thick paraffin sections. Results are expressed as mean ± standard deviation.

These data suggest that IL-1β does not affect oligodendrocyte proliferation or survival but rather affects maturation, with potentially a partial blockade at the transition between oligodendrocyte progenitor and precursor.

FIGURE 7: The systemic injection of interleukin (IL)-1β from P1 to P5 led to a significant increase of oligodendrocyte progenitors associated with a reduction of mature oligodendrocytes. (A) Immunofluorescent staining of NG2/DAPI, performed on frozen sections, within the external capsule of P5 mice treated with phosphate-buffered saline (PBS) or IL-1β from P1 to P5 (original low magnification ×40, scale bar = 50μm; high magnification ×63, scale bar = 10μm). (B) Quantification of fluorescent NG2$^+$ cells/mm^2 at P5, P10, P15, and P30 within the external capsule of mice treated with PBS (n = 6 at each age, *white bars*) or IL-1β (n = 6 at each age, *black bars*). (C) Relative quantification of the PDGFRα transcript within cortex and white matter at P0 (n = 4, *gray bar*) and at P5, P10, P15, and P30 in mice treated with PBS (n = 4 at each age, *white bars*) or IL-1β (n = 4 at each age, *black bars*). (D, E) Immunofluorescent stainings of PDGFRα (green)/DAPI (D) and of O4 (red)/DAPI (E) on 10μm-thick frozen sections, within the external capsule of P5 mice treated with either PBS or IL-1β from P1 to P5 (original low magnification ×40, scale bar = 50μm; original high magnification ×63, scale bar = 10μm). Quantification of fluorescent PDGFRα^+ (D) and O4$^+$ (E) cells/mm^2 within the external capsule of mice treated with PBS (n = 6, *white bars*) or IL- 1β (n = 6, *black bars*) at P5. (F) Assessment of 2′3′cyclic nucleotide 3′ phosphohydrolase (CNPase) gene expression by quantitative polymerase chain reaction within cortex and white matter at P0 (n = 4, *gray bar*) and at P5, P10, P15, and P30 in mice treated with PBS (n = 4 at each age, *white bars*) or IL-1β (n = 4 at each age, *black bars*). (G) Photomicrographs of the Adenomatosis Polyposis Coli (APC) immunostaining at the external capsule level at P15 performed on 10μm-thick paraffin sections (original magnification ×20, scale bars = 100μm). (H) Quantification of APC$^+$ cells/mm^2 within the external capsule at P10, P15, and P30 in mice treated with PBS (n = 6 at each age, *white bars*) or IL-1β (n = 6 at each age, *black bars*) from P1 to P5. Results are expressed as mean ± standard deviation. Asterisks indicate statistically significant difference from white bar, *$p < 0.05$, **$p < 0.01$, and ***$p < 0.001$ by Mann-Whitney test.

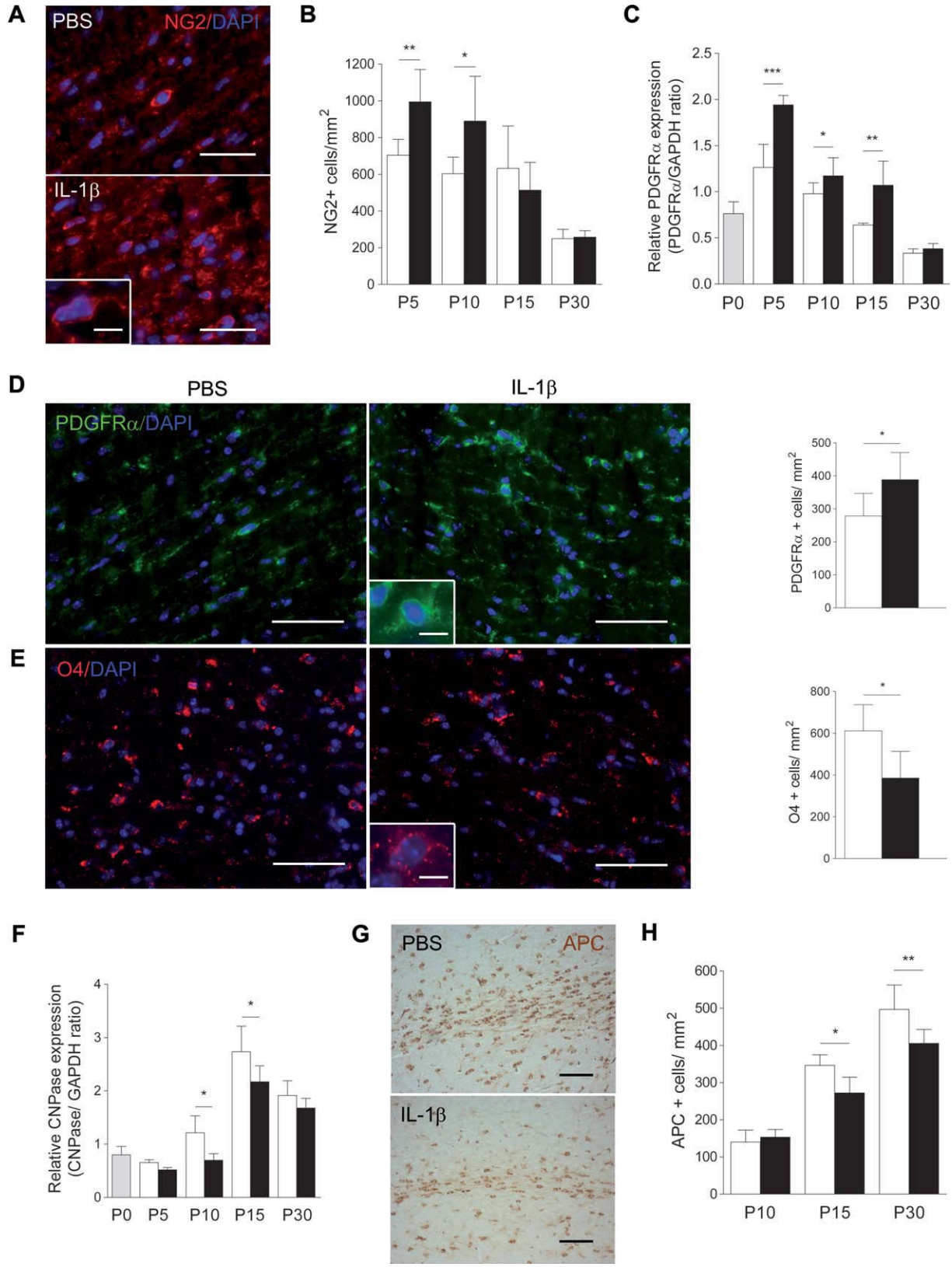
A
PBS
NG2/DAPI
IL-1β
B
NG2+ cells/mm2
P5
P10
P15
P30
C
Relative PDGFRα expression (PDGFRα/GAPDH ratio)
P0
P5
P10
P15
P30
D
PBS
IL-1β
PDGFRα/DAPI
PDGFRα + cells/ mm2
E
O4/DAPI
O4 + cells/ mm2
F
Relative CNPase expression (CNPase/ GAPDH ratio)
P0
P5
P10
P15
P30
G
PBS
APC
IL-1β
H
APC + cells/ mm2
P10
P15
P30

FIGURE 7.

IL-1β Disrupted the Machinery Controlling Oligodendrocyte Maturation

To explore this further, we performed real time reverse transcription PCR (RT-PCR) of transcription factors known to be involved in the maturation/differentiation process of oligodendrocytes. Wheras expression of Olig1, Olig2, Sox10, Tcf4, Axin2, HDAC1, and HDAC3 was increased, that of Nkx2.2, Sox8, and P27Kip1 was inhibited after IL-1β treatment (Fig 8).

The expression of factors known to mediate the interactions between axons and oligodendrocytes was also measured by real time RT-PCR. No significant effect of IL-1β was detected on the expression of SemaphorinA3, PlexinA4, EphrinB2, EphrinB3, Fyn, Lingo1, and Neuregulin1 and its receptors ErbB2 and ErbB4 (Supplementary Fig 6).

IL-1β Did Not Have a Major Impact on Other Cell Types

IL-1β injections between P1 and P5 had no detectable effect on neocortical cell death (cleaved caspase 3 immunostaining), neuronal density (NeuN immunostaining), and astrocyte density (glial fibrillary acidic protein immunostaining) (Supplementary Fig 7A–C). In contrast, IL-1β injections between P1 and P5 induced a transient increase in the density of microglia in the neopallium (MAC1 and Iba-1 immunostaining) (Supplementary Fig 7D–E).

Discussion

We have shown that a moderate systemic inflammatory stimulus disrupts oligodendrocyte and axon maturation, and impairs myelination in newborn mice. This long-lasting myelination defect is accompanied by abnormal FA on DTI and cognitive behavioral defects.

Neonatal Systemic Inflammation Disrupts White Matter Programming

In the present model, no obvious brain lesion or neural cell death was detected, strongly suggesting that white matter abnormalities were the result of alterations of the developmental program of the brain. In keeping with this hypothesis, the expression of several factors involved in oligodendrocyte and axon maturation was altered following systemic inflammation. In addition, myelination defects were observed when pups were exposed to systemic inflammation between P1 and P5 but not when they were exposed between P6 and P10, suggesting a period of vulnerability of the developing white matter. As developmental events occurring at P1 are quite different from those occurring at P5, further studies will be necessary to potentially refine the window of vulnerability, specifically, to determine if repeated exposures in the P1 to P5 period are required to produce this myelination defect or if exposure to IL-1β at a given day is sufficient.

White Matter Disease Is Both an Oligopathy and an Axonopathy

Although research has identified damage to oligodendrocytes as the cause of periventricular white matter damage in the human preterm infant,[27] the potential specific contribution of axonopathy to white matter abnormalities and dysfunction remains to be clarified.[28] This is critical, as axonopathies have been described in a variety of other human diseases affecting the white matter, such as multiple sclerosis[29] and leukodystrophies.[30]

In the present model, a combination of markers suggests a block of oligodendrocyte maturation at the progenitor stage, whereas proliferation and survival remained unaffected. Although the precise mechanisms linking systemic inflammation and blockade of oligodendrocyte maturation will require further studies, the present data suggest an imbalance between transcription factors controlling oligodendrocyte maturation. Indeed, some transcriptional factors known to play a role during oligodendrocyte maturation/differentiation, such as Olig1,[31] Olig2,[32] Sox10,[33] Tcf4,[34] Axin2, HDAC1,[35] and HDAC3,[36] are increased by systemic IL-1β, whereas other transcription factors also involved in oligodendrocyte maturation, such as Nkx2.2[37] and Sox8,[38] are reduced.

In addition to the oligopathy, we observed a clear axonopathy by electron microscopy, with reduced diameter of myelinated axons, and altered water diffusivity on DTI in IL-1β-exposed animals. IL-1β also significantly inhibited the expression of Wnt7a, a transcription factor involved in axonal maturation,[25,26] supporting evidence of an axonopathy.

Interactions between oligodendrocytes and axons are important for oligodendrocyte maturation, axonal growth, and myelination.[39] Thus, inflammation-induced axonopathy due to systemic IL-1β may disrupt these interactions, leading to abnormal white matter. The analysis at the transcription level of some factors known to mediate these interactions, such as Semaphorin3a, PlexinA4, EphrinB2,[40] EphrinB3,[41] Fyn,[42] Lingo1,[43] and Neuregulin1 and its receptors ErbB2 and ErbB4,[44,45] did not reveal any significant effect of IL-1β. Interestingly, although IL-1β exposure between P6 and P10 did not interfere with myelination, it had a significant impact on the expression of Wnt7a and light chain neurofilament, suggesting that the effects of IL-1β on myelination and on axonal growth might be partly dissociated.

Interestingly, at the electron microscopic level in IL-1β–treated animals, a large number of axons were totally deprived of myelin, whereas other axons had normally compacted myelin. The mechanisms and

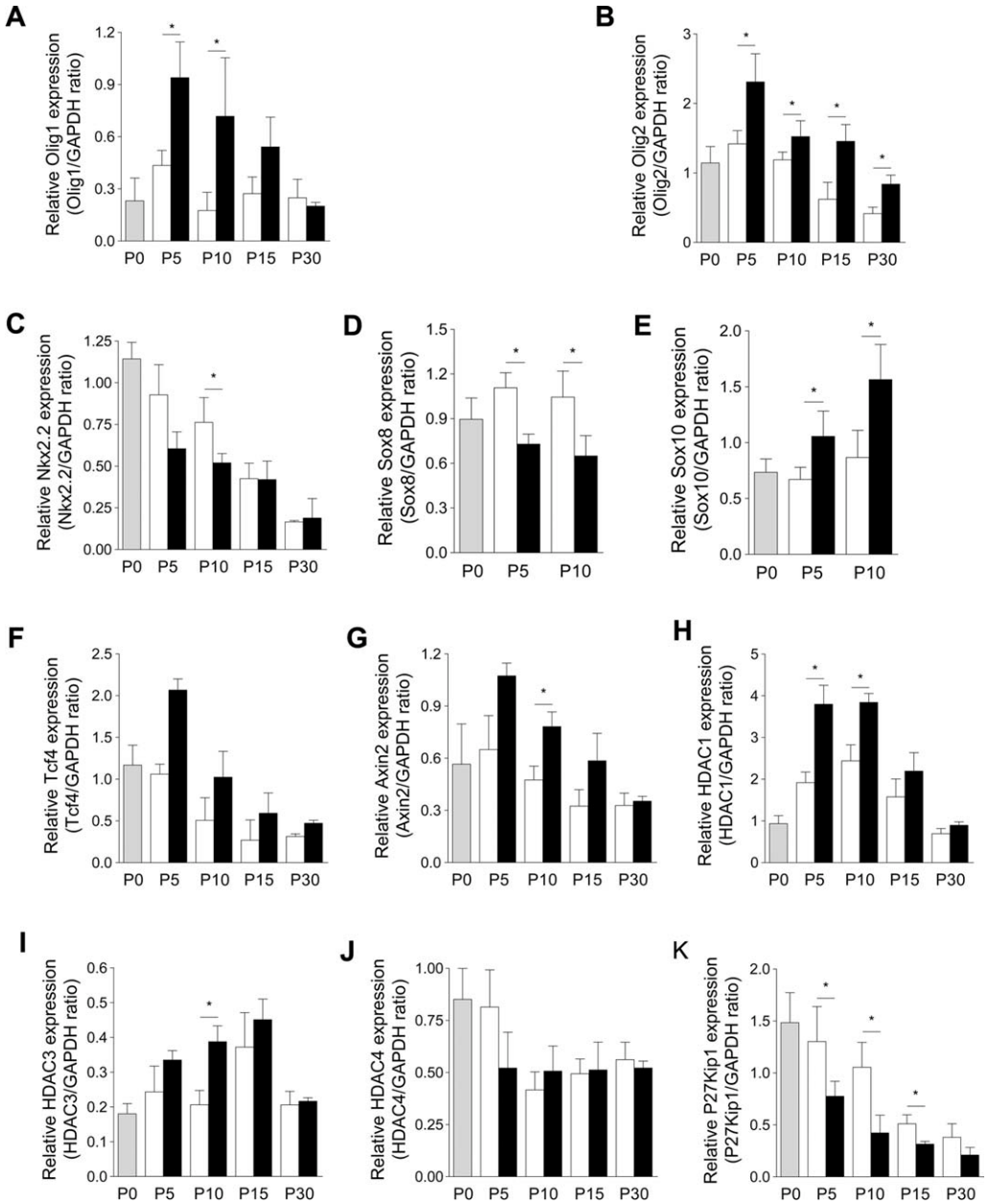

FIGURE 8: The systemic injection of interleukin (IL)-1β from P1 to P5 perturbed the expression of key factors involved in oligodendrocyte maturation. Relative gene expression of Olig1 (A), Olig2 (B), Nkx2.2 (C), Sox8 (D), Sox10 (E), Tcf4 (F), Axin2 (G), HDAC1 (H), HDAC3 (I), HDAC4 (J), and P27Kip1 (K) were assessed by quantitative polymerase chain reaction within cortex and white matter at P0 (n = 4, *gray bars*) and at P5, P10, P15, and P30 in mice treated with phosphate-buffered saline (n = 4 at each age, *white bars*) and with IL-1β (n = 4 at each age, *black bars*). Results are expressed as mean ± standard deviation. Asterisks indicate statistically significant difference from white bar, *$p < 0.05$ by Mann-Whitney test.

functional significance of this phenomenon remain elusive and warrant further investigation.

Clinical Relevance of the Present Model

The relevance of our model for understanding white matter disease of human preterm infants is supported by several observations from this study.

First, the apparently moderate intensity of this inflammatory insult compared to other models based on LPS or *E. coli* administration[13,46] adds to its relevance to clinically silent or minor chorioamnionitis often observed in preterm infants.

Second, the systemic inflammation is accompanied by moderate but significant effects on ventilation and temperature, which are reminiscent of what is observed in preterm infants exposed to chorioamnionitis.[47]

Third, our MRI findings are consistent with white matter abnormalities described in recent imaging studies in

very preterm infants also without detectable tissue destruction on anatomical sequences.[48] In the present study, the observed FA reduction, mainly due to an increase of $D_{\perp}$, suggests a selective alteration of white matter, as a result of myelination deficit and/or of myelin sheath damage.

Additionally, behavioral testing of adult animals exposed to neonatal inflammation revealed significant cognitive deficits but no motor impairment, similar to the neurobehavioral profile observed in recent follow-up cohorts of very preterm infants.[3] Of note, although the novel object and displaced object recognition tests are generally considered as testing hippocampal functions, memory requires structures beyond the hippocampus. Illustrating this, we have shown that cortical and white matter lesions induced by glutamate analog injection into the neopallium are sufficient to impair performances in these tests.[49]

Despite this relevance of our model, when extrapolating the present observations to the human situation it is important to remember species differences in inflammatory mechanisms. Nevertheless, increased IL-1β is a common hallmark of inflammation/infection in humans and mice,[50,51] supporting the use of our model to further the understanding of white matter disease.

To our knowledge, this is the first study showing that a moderate systemic inflammation occurring at a specific time during the perinatal period can alter the developmental programs of the white matter. This insult leads to a long-lasting myelination deficit accompanied by cognitive defects, mimicking MRI abnormalities and neurological handicaps observed in some human preterm infants. The impact of perinatal inflammation on programs of brain development could also have long-term consequences in terms of susceptibility to adult brain diseases.

Acknowledgments

This study was supported by grants from Inserm (P.G.), Paris Diderot University (P.G.), Assistance Publique des Hôpitaux de Paris (Public Parisian Hospitals; Interface contract to P.G.), PremUP Foundation (P.G.), Sixth Framework Program of the European Commission (contract No. LSHM-CT-2006-036534/NEOBRAIN; P.G., O.D., H.H.), Seventh Framework Program of the European Union (contract No. HEALTH-F2-2009-241778/NEUROBID; P.G., O.D.), Leducq Foundation (P.G., H.H.), European Leukodystrophy Association (G.F., P.G.), Société Frančaise de Pédiatrie (French Society for Pediatrics; G.F.), Journées Francophones de Recherche en Néonatologie (G.F.), Fondation pour le Recherche Médicale (Medical Research Foundation), Swiss National Fund (31003A-112233; S.S.), Biomedical Imaging Centre of the Geneva University (UNIGE), Lausanne University (UNIL), Geneva University Hospital (HUG), Lausanne University Hospital (CHUV), Lausanne Polytechnic School (EPFL), Leenards and Jeantet Foundations (Y.v.d.L., S.S.), Swedish Medical Research Council (VR 2006-3396; H.H.), Swedish governmental grants to researchers in the public health service (ALFGBG2863; H.H.), Medical Research Council UK (P19381; H.H.), Medical Research Council Sweden (H.H.), and Action Medical Research UK (SP4506; H.H.).

We thank F. Cluzeaud for excellent assistance with the electron microscopy.

Authorship

V.L. and P.G. contributed equally to the work.

Potential Conflicts of Interest

Nothing to report.

References

1. Larroque B, Ancel PY, Marret S, et al. Neurodevelopmental disabilities and special care of 5-year-old children born before 33 weeks of gestation (the EPIPAGE study): a longitudinal cohort study. Lancet 2008;371:813–820.
2. Wilson-Costello D, Friedman H, Minich N, et al. Improved neurodevelopmental outcomes for extremely low birth weight infants in 2000–2002. Pediatrics 2007;119:37–45.
3. Delobel-Ayoub M, Arnaud C, White-Koning M, et al. Behavioral problems and cognitive performance at 5 years of age after very preterm birth: the EPIPAGE Study. Pediatrics 2009;123:1485–1492.
4. Volpe JJ. Cerebral white matter injury of the premature infant—more common than you think. Pediatrics 2003;112:176–180.
5. Dammann O, Leviton A. Inflammatory brain damage in preterm newborns—dry numbers, wet lab, and causal inferences. Early Hum Dev 2004;79:1–15.
6. Wu YW, Colford JM Jr. Chorioamnionitis as a risk factor for cerebral palsy: a meta-analysis. JAMA 2000;284:1417–1424.
7. Nelson KB, Grether JK, Dambrosia JM, et al. Neonatal cytokines and cerebral palsy in very preterm infants. Pediatr Res 2003;53:600–607.
8. Bartha AI, Foster-Barber A, Miller SP, et al. Neonatal encephalopathy: association of cytokines with MR spectroscopy and outcome. Pediatr Res 2004;56:960–966.
9. Eklind S, Mallard C, Leverin AL, et al. Bacterial endotoxin sensitizes the immature brain to hypoxic–ischaemic injury. Eur J Neurosci 2001;13:1101–1106.
10. Dommergues MA, Patkai J, Renauld JC, et al. Proinflammatory cytokines and interleukin-9 exacerbate excitotoxic lesions of the newborn murine neopallium. Ann Neurol 2000;47:54–63.
11. Malaeb S, Dammann O. Fetal inflammatory response and brain injury in the preterm newborn. J Child Neurol 2009;24:1119–1126.
12. Volpe JJ. Brain injury in premature infants: a complex amalgam of destructive and developmental disturbances. Lancet Neurol 2009;8:110–124.
13. Debillon T, Gras-Leguen C, Verielle V, et al. Intrauterine infection induces programmed cell death in rabbit periventricular white matter. Pediatr Res 2000;47:736–742.

14. Normann E, Lacaze-Masmonteil T, Eaton F, et al. A novel mouse model of Ureaplasma-induced perinatal inflammation: effects on lung and brain injury. Pediatr Res 2009;65:430–436.
15. Rousset CI, Chalon S, Cantagrel S, et al. Maternal exposure to LPS induces hypomyelination in the internal capsule and programmed cell death in the deep gray matter in newborn rats. Pediatr Res 2006;59:428–433.
16. Bollen B, Bouslama M, Matrot B, et al. Cold stimulates the behavioral response to hypoxia in newborn mice. Am J Physiol Regul Integr Comp Physiol 2009;296:R1503–R1511.
17. Lofaso F, Dauger S, Matrot B, et al. Inhibitory effects of repeated hyperoxia on breathing in newborn mice. Eur Respir J 2007;29:18–24.
18. Matrot B, Durand E, Dauger S, et al. Automatic classification of activity and apneas using whole body plethysmography in newborn mice. J Appl Physiol 2005;98:365–370.
19. Ramanantsoa N, Vaubourg V, Matrot B, et al. Effects of temperature on ventilatory response to hypercapnia in newborn mice heterozygous for transcription factor Phox2b. Am J Physiol Regul Integr Comp Physiol 2007;293:R2027–R2035.
20. Dingley J, Hobbs C, Ferguson J, et al. Xenon/hypothermia neuroprotection regimes in spontaneously breathing neonatal rats after hypoxic-ischemic insult: the respiratory and sedative effects. Anesth Analg 2008;106:916–923.
21. Bonnin P, Debbabi H, Mariani J, et al. Ultrasonic assessment of cerebral blood flow changes during ischemia-reperfusion in 7-day-old rats. Ultrasound Med Biol 2008;34:913–922.
22. Olivier P, Baud O, Evrard P, et al. Prenatal ischemia and white matter damage in rats. J Neuropathol Exp Neurol 2005;64: 998–1006.
23. Deprez M, Ceuterick-de Groote C, Fumal A, et al. A new combined Bodian-Luxol technique for staining unmyelinated axons in semithin, resin-embedded peripheral nerves: a comparison with electron microscopy. Acta Neuropathol 1999;98:323–329.
24. Favrais G, Schwendimann L, Gressens P, Lelievre V. Cyclooxygenase-2 mediates the sensitizing effects of systemic IL-1-beta on excitotoxic brain lesions in newborn mice. Neurobiol Dis 2007;25: 496–505.
25. Shimogori T, VanSant J, Paik E, Grove EA. Members of the Wnt, Fz, and Frp gene families expressed in postnatal mouse cerebral cortex. J Comp Neurol 2004;473:496–510.
26. Hirabayashi Y, Itoh Y, Tabata H, et al. The Wnt/beta-catenin pathway directs neuronal differentiation of cortical neural precursor cells. Development 2004;131:2791–2801.
27. Volpe JJ. Neurobiology of periventricular leukomalacia in the premature infant. Pediatr Res 2001;50:553–562.
28. Leviton A, Gressens P. Neuronal damage accompanies perinatal white-matter damage. Trends Neurosci 2007;30:473–478.
29. Piaton G, Gould RM, Lubetzki C. Axon-oligodendrocyte interactions during developmental myelination, demyelination and repair. J Neurochem 2010;114:1243–1260.
30. Hofling AA, Kim JH, Fantz CR, et al. Diffusion tensor imaging detects axonal injury and demyelination in the spinal cord and cranial nerves of a murine model of globoid cell leukodystrophy. NMR Biomed 2009;22:1100–1106.
31. Xin M, Yue T, Ma Z, et al. Myelinogenesis and axonal recognition by oligodendrocytes in brain are uncoupled in Olig1-null mice. J Neurosci 2005;25:1354–1365.
32. Liu Z, Hu X, Cai J, et al. Induction of oligodendrocyte differentiation by Olig2 and Sox10: evidence for reciprocal interactions and dosage-dependent mechanisms. Dev Biol 2007;302:683–693.
33. Wei Q, Miskimins WK, Miskimins R. Sox10 acts as a tissue-specific transcription factor enhancing activation of the myelin basic protein gene promoter by p27Kip1 and Sp1. J Neurosci Res 2004;78:796–802.
34. Fancy SP, Baranzini SE, Zhao C, et al. Dysregulation of the Wnt pathway inhibits timely myelination and remyelination in the mammalian CNS. Genes Dev 2009;23:1571–1585.
35. Ye F, Chen Y, Hoang T, et al. HDAC1 and HDAC2 regulate oligodendrocyte differentiation by disrupting the beta-catenin-TCF interaction. Nat Neurosci 2009;12:829–838.
36. Shen S, Li J, Casaccia-Bonnefil P. Histone modifications affect timing of oligodendrocyte progenitor differentiation in the developing rat brain. J Cell Biol 2005;169:577–589.
37. Zhou Q, Choi G, Anderson DJ. The bHLH transcription factor Olig2 promotes oligodendrocyte differentiation in collaboration with Nkx2.2. Neuron 2001;31:791–807.
38. Stolt CC, Lommes P, Friedrich RP, Wegner M. Transcription factors Sox8 and Sox10 perform non-equivalent roles during oligodendrocyte development despite functional redundancy. Development 2004;131:2349–2358.
39. Nave KA, Trapp BD. Axon-glial signaling and the glial support of axon function. Annu Rev Neurosci 2008;31:535–561.
40. Yiu G, He Z. Glial inhibition of CNS axon regeneration. Nat Rev Neurosci 2006;7:617–627.
41. Xiao Q, Chen J, Wu YQ. Expression of ephrin-B3 mRNA and cellular apoptosis in the brain of neonatal rats with periventricular leukomalacia. Zhongguo Dang Dai Er Ke Za Zhi 2007;9: 321–323.
42. Sperber BR, Boyle-Walsh EA, Engleka MJ, et al. A unique role for Fyn in CNS myelination. J Neurosci 2001;21:2039–2047.
43. Mi S, Lee X, Shao Z, et al. LINGO-1 is a component of the Nogo-66 receptor/p75 signaling complex. Nat Neurosci 2004;7:221–228.
44. Brinkmann BG, Agarwal A, Sereda MW, et al. Neuregulin-1/ErbB signaling serves distinct functions in myelination of the peripheral and central nervous system. Neuron 2008;59:581–595.
45. Dammann O, Bueter W, Leviton A, et al. Neuregulin-1: a potential endogenous protector in perinatal brain white matter damage. Neonatology 2008;93:182–187.
46. Young RS, Yagel SK, Towfighi J. Systemic and neuropathologic effects of E. coli endotoxin in neonatal dogs. Pediatr Res 1983;17: 349–353.
47. Abu-Shaweesh JM, Martin RJ. Neonatal apnea: what's new? Pediatr Pulmonol 2008;43:937–944.
48. Brown NC, Inder TE, Bear MJ, et al. Neurobehavior at term and white and gray matter abnormalities in very preterm infants. J Pediatr 2009;155:32–38, 38.e31.
49. Titomanlio L, Bouslama M, Verche VL, et al. Implanted neurosphere-derived precursors promote recovery after neonatal excitotoxic brain injury. Stem Cells Dev 2011;20:865–879.
50. Gotsch F, Romero R, Kusanovic JP, et al. The fetal inflammatory response syndrome. Clin Obstet Gynecol 2007;50:652–683.
51. Feuerstein GZ, Wang X, Barone F. Inflammatory gene expression in cerebral ischemia and trauma. Ann N Y Acad Sci 1997;825: 179–193.